© UNIVERSAL RESEARCH REPORTS | REFEREED | PEER REVIEWED
ISSN : 2348 - 5612 | Volume : 05 , Issue : 02 | January – March 2018

Synthesis, Characterization and Luminescent features of $Ca_{1-x}ZrO_3$: xDy^{3+} Nanophosphors

Sonika Singh[1], S.P. Khatkar[1], Rajesh Kumar[2], Sheetal[1], V.B. Taxak[1*]
[1]Department of Chemistry, Maharshi Dayanand University, Rohtak-124001, India
[2]Department of Applied Sciences, UIET, Maharshi Dayanand University, Rohtak-124001, India

Abstract : $Ca_{1-x}ZrO_3$: xDy^{3+} nanophosphors have been successfully synthesized using urea assisted solution combustion route. X-ray diffraction (XRD), scanning electron microscopy (SEM) and transmission electron microscopy (TEM) were done to study the structural features of Dy^{3+} doped $CaZrO_3$ nanophosphor. The results of XRD patterns indicate that $Ca_{1-x}Dy_xZrO_3$ nanophosphors crystallize in pure orthorhombic pervoskite structure having space group *Pnma* (62) at 1200°C. SEM and TEM analysis revealed smooth slightly agglomerated spherical morphology particles having size in diameter range 50 – 60 nm. Luminescent properties were investigated by measuring excitation and emission spectra with decay curves of $Ca_{1-x}Dy_xZrO_3$ nanophosphors. The photoluminescence (PL) spectra of $Ca_{1-x}Dy_xZrO_3$ nanophosphors consist of two sharp emission lines in the blue region (470-490 nm) and yellow region (530-650 nm), monitored at 353 nm excitation. The blue emission centered at 484 nm corresponds to $^4F_{9/2}\rightarrow{}^6H_{15/2}$ while yellow emission with maxima at 576 nm is ascribed $^4F_{9/2}\rightarrow{}^6H_{13/2}$ transitions of Dy^{3+} ions, respectively. Luminescence concentration quenching could be observed when the doping concentration of Dy^{3+} ions was more than 4 mol%. $Ca_{1-x}Dy_xZrO_3$ nanophosphors exhibit bright luminescence in the white region that makes it an excellent candidate for new lighting devices.

ISSN : 2348-5612 © URR
9 770234 856124

Keywords: Nanophosphor ● Combustion ● Luminescent ● $Ca_{1-x}Dy_xZrO_3$

Introduction : Metal oxides ABO_3 (where A = Ca, Pb, Sr, Ba, Zn, Ni, Fe; B = Ti, Zr, Si, Hf) with perovskite structure have attracted significant attention owing to their superconductivity and remarkable electrical properties such as ferroelctricity and piezoelectricity [1-5]. Alkaline-earth zirconates are well known for their structural diversity including high thermal and chemical stability, single phase crystalline structure, high refractive index and wide band gap which results in their potential technological applications in electronic ceramic industry, gas sensors, optical coatings, filters and so on [6-8]. Among the perovskite zirconates $CaZrO_3$, seems to be considerably important for both mechanical and electrical applications due to its high permittivity, insulation resistance, high ionic conductivity, good corrosion resistance, hydrocarbon sensing and high thermal sensitivity [9-16]. In addition, ABO_3 perovskites doped with acceptor-ions exhibits proton conductivity at high temperature, making them suitable for electrochemical devices [17].

A perovskite ABO_3 lattice consists of slightly deformed BO_6 octahedra with B-O-B angles at 180° and 12-oxygen coordinated A^{2+} cations with m3m symmetry at dodecahedral site. Calcium zirconate oxide appears to be potential host matrix as it possesses most distorted structure favorable for the doping of trivalent rare earth ions (RE^{3+}) [18]. Rare earth ions are known for their excellent luminescent properties when doped in different inorganic host lattices. Among the RE^{3+} ions, Dy^{3+} ions exhibits strong

luminescence in a variety of host lattices and show characteristic both blue ($^4F_{9/2} \rightarrow {}^6H_{15/2}$) and yellow ($^4F_{9/2} \rightarrow {}^6H_{13/2}$) emissions, necessary for generation of white light very useful for high resolution optical display system [19-22]. However, only limited information regarding the doping of dysprosium ions in calcium zirconate perovskite oxide are available in the literature. In the past, sol-gel process has been exploited to synthesize $CaZrO_3:Dy^{3+}$ phosphor and the photoluminescence properties of Dy^{3+} and Tm^{3+} co-activated $CaZrO_3$ phosphor were investigated [23-24]. But no reports on the solution combustion synthesis of Dy^{3+} doped $CaZrO_3$ nano-crystalline phosphors has come into the notice. The present work reports synthesis and characterization of $CaZrO_3$: Dy^{3+} using urea assisted solution combustion process. Moreover, dependence of structural and photoluminescence properties of these nanophosphors on various parameters such as temperature and dysprosium stoichiometry have also been studied in details.

A. EXPERIMENTAL

i) Powder Synthesis

$Ca_{1-x}ZrO_3$: xDy^{3+} nanophosphors were synthesized by solution combustion method using high purity $Ca(NO_3)_2.4H_2O$, ZrN_2O_7, $Dy(NO_3)_3.6H_2O$ and urea as starting reagents. The chemical equation for the reactions is:

$(1-x)Ca(NO_3)_2 + xDy(NO_3)_3 + ZrN_2O_7 + \sim 3.5\ CH_4N_2O \rightarrow Ca_{1-x}Dy_xZrO_3$ (s) + gaseous products.

According to nominal composition of $Ca_{1-x}ZrO_3$: xDy^{3+} (x = 0.01 to 0.05), a stoichiometric amount of metal nitrates were dissolved in minimum quantity of deionized water in 200 mL capacity pyrex beaker. Then urea was added in this solution with molar ratio of urea to oxidizer based on total oxidizing and reducing valencies of oxidizer and fuel (urea) according to concept used in propellant chemistry [25]. This aqueous paste containing calculated amount of metal nitrates and urea was then placed in a preheated furnace maintained at 500°C. The mixture of metal nitrates (oxidizers) and fuel (urea) undergo rapid and self-sustaining combustion process and the chemical energy released during this exothermic redox reaction results in dehydration and foaming followed by decomposition. Consequently, the large amounts of volatile combustible gases generated alongwith flames, yields voluminous solid within 5-8 minutes. The powders obtained were again fired from 800°C to 1200°C for 3h in order to evaluate the effect of sintering on the structural and luminescent features on $Ca_{1-x}ZrO_3$: xDy^{3+} nanophosphors.

ii) Powder Characterization Techniques

Crystal phase and particle size of $CaZrO_3$: Dy^{3+} powders were examined by Rigaku Ultima-IV X-ray powder diffractometer with CuKα radiation to record the patterns in 2θ range of 20°-65°. Surface morphology was evaluated using Jeol JSM-6510 scanning electron microscope. The surface morphology of the samples was examined using Jeol JSM-6510 scanning electron microscope (SEM). The crystallite size and shape has been evaluated using Tecnai G^2 transmission electron microscope (TEM). The photoluminescence excitation and emission in the ultraviolet-visible region and decay curves under time scan mode were carried out on Hitachi F-7000 fluorescence spectrophotometer equipped with Xe-lamp at room temperature.

B. RESULTS AND DISCUSSION

i) X-ray Studies

$CaZrO_3$ is one of the most distorted orthorhombic perovskite structures where divalent Ca cation occupies distorted dodecahedral site. In this perovskite lattice, rotation of slightly deformed ZrO_6 octahedra distorts the Ca^{2+} site causing reduction in its symmetry site from Pm3m to 1 along with decrease in coordination from 12 to 8 [23]. On introducing in $CaZrO_3$ host, the dopant Dy^{3+} (0.092 nm) has a single choice between substitution sites of Ca^{2+} ion (0.099 nm) and Zr^{4+} (0.072 nm) due to comparable ionic size difference, hence preferably substitute Ca^{2+} site in this lattice. XRD patterns of $Ca_{0.96}Dy_{0.04}ZrO_3$ nanophosphor as-synthesized and sintered at different temperatures from 800°C to 1200°C alongwith the standard JCPDS No. 35-0790 are represented in Fig.1a. At 1200°C, $Ca_{0.96}Dy_{0.04}ZrO_3$ nanophosphor crystallizes in pure orthorhombic pervoskite structure having space group *Pnma* (62) and lattice parameters a = 5.755, b = 8.010 and c = 5.592 belonging to JCPDS No. 35-0790. The main diffraction peaks at 22.12° (101), 24.76° (111), 31.02° (200), 31.49° (121), 31.92° (002), 37.27° (031), 45.13° (202), 50.17° (301), 50.81° (222), 51.49° (103), 55.47° (321), 55.79° (240), 56.38° (042), 56.64° (123) and 65.74° (242) due to orthorhombic $CaZrO_3$ lattice were observed. No traces of other peaks due to additional phases apart from single pervoskite $CaZrO_3$ phase was detected at this temperature. While at lower temperatures, weak reflex lines of ZrO_2 (JCPDS No.49-1746) marked as '*' were also apparent alongwith all the main diffraction peaks of $CaZrO_3$. The XRD profiles of the $Ca_{0.96}Dy_{0.04}ZrO_3$ nanophosphors at lower temperatures (800°C and 1000°C) indicated a high degree of peak broadening which shows that sample is amorphous with only weak evidence of crystallinity. It is clearly seen that on increasing the temperature, the intensity of main peak (121) plane enhanced with the decrease in line width, concluding that the crystalline degree of dysprosium doped $CaZrO_3$ nanocrystals is improved apparently with the rise in sintering temperature.

The XRD patterns of $Ca_{(1-x)}Dy_xZrO_3$ powders sintered at 1200°C, doped with different contents of dysprosium ions alongwith the standard JCPDS No. 35-0790 are depicted in Fig.1b. It is quite evident that all the samples exhibit single orthorhombic $CaZrO_3$ phase belonging to space group *Pnma*, indicating small amount of doped Dy^{3+} ions had no influence on crystal structure of this lattice. The crystallite size, D of $Ca_{(1-x)}ZrO_3 : xDy^{3+}$ powders was estimated by Scherrer's formula, $D = 0.941\lambda/\beta \cos\theta$, where λ is the wavelength of CuKα radiation (0.1548 nm), β is the full width in radians at half-maximum (FWHM) and θ is the Bragg's angle of an observed X-ray diffraction peak. The calculated average crystallite sizes, by taking main peak (121) of $Ca_{0.96}Dy_{0.04}ZrO_3$ powders came out to be 45.3 nm, 53.2 and 64.5 nm due to pervoskite $CaZrO_3$ phase as-synthesized, at sintering temperatures 800°C, 1000°C and 1200°C, respectively. It was observed that all the powders are in nano-regime range although an increase in particle size with the rise in sintering temperature was noticed due to enhanced atomic mobility of particles which leads to faster grain growth at higher temperature.

© UNIVERSAL RESEARCH REPORTS | REFEREED | PEER REVIEWED
ISSN : 2348 - 5612 | Volume : 05 , Issue : 02 | January – March 2018

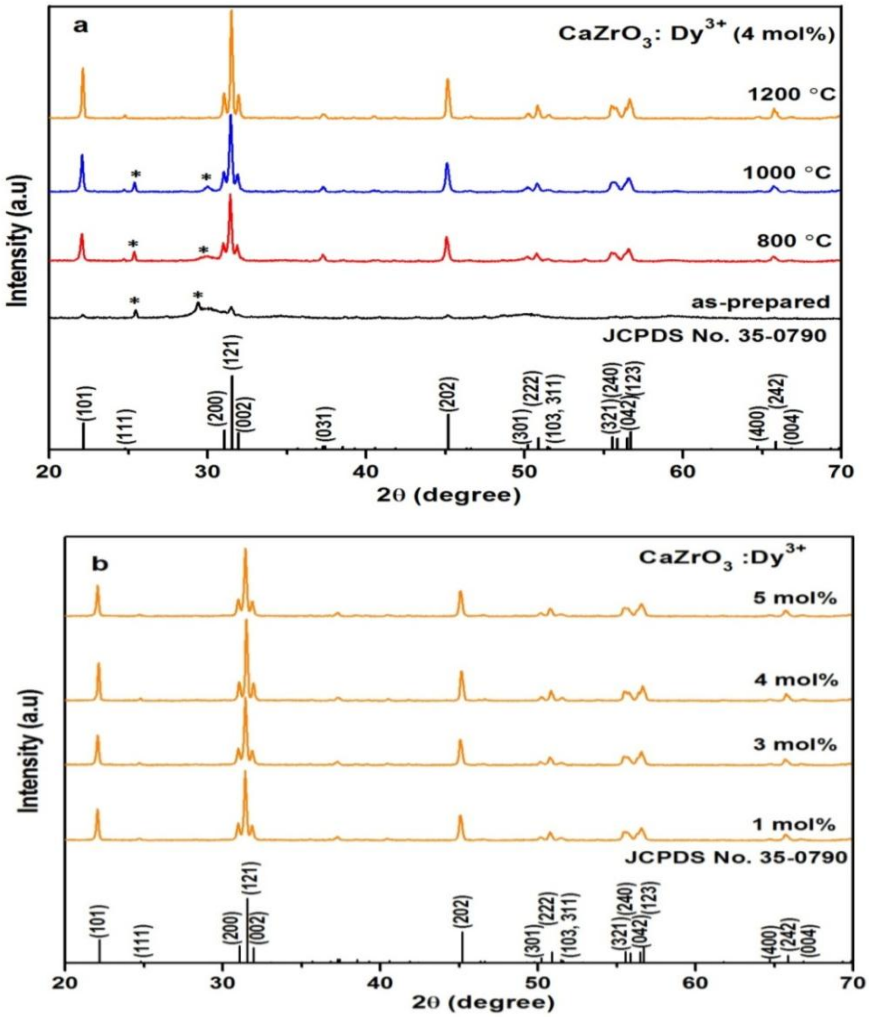

Fig.1. XRD patterns of (a) $Ca_{0.96}Dy_{0.04}ZrO_3$ powders sintered at various temperatures (b) $Ca_{1-x}Dy_xZrO_3$ (x = 1 to 5 mol%), sintered at 1200°C along with standard data of $CaZrO_3$ (JCPDS no. 35-0790).

ii) Morphological Characteristics

SEM and TEM studies were carried out to investigate the morphology and particle size of the dysprosium doped $CaZrO_3$ nanophosphors. SEM image of $Ca_{0.96}Dy_{0.04}ZrO_3$ powder sintered at 1200°C clearly depicts narrow size distribution of slightly agglomerated spherical shaped particles (Fig..2).

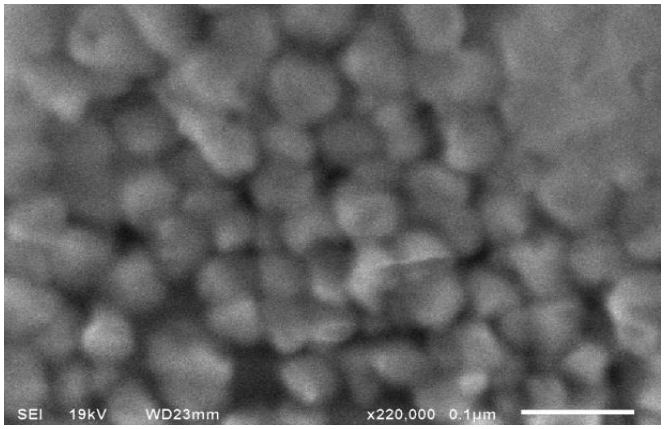

Fig. 2 SEM micrographs of $Ca_{0.96}Dy_{0.04}ZrO_3$ powders sintered at 1200°C

TEM image of $Ca_{0.96}Dy_{0.04}ZrO_3$ powder sintered at 1200°C also show smooth slightly agglomerated spherical morphology particles having size in diameter range 50 - 60 nm (Fig. 3). The particle size estimation from TEM studies is well consistent with that of XRD results.

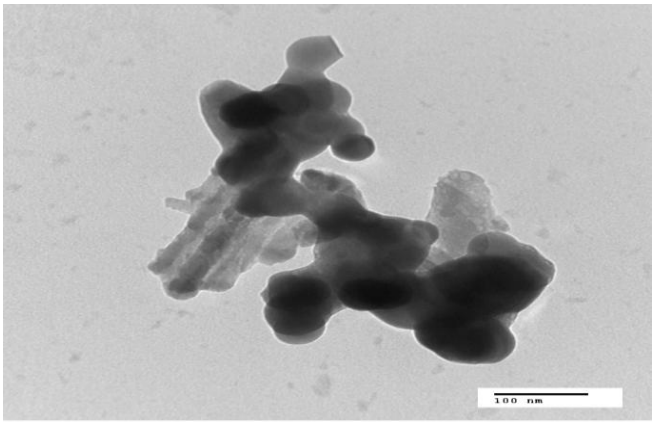

Fig. 3 TEM micrograph of $Ca_{0.96}Dy_{0.04}ZrO_3$ powders sintered at 1200°C.

iii) Luminescent Studies

The photoluminescence excitation (PLE) spectrum of $Ca_{0.96}Dy_{0.04}ZrO_3$ nanophosphors sintered at 1200°C, monitored with yellow emission, 576 nm corresponding to $^4F_{9/2} \rightarrow {}^6H_{13/2}$ transition in 200-500 nm range is shown in Fig. 4. The PLE spectrum can be divided into a very weak broad band in the ultraviolet region (200-275 nm) with a maximum at 258 nm, which might be overlapping of attributed to charge transfer states (CTS) due to $O^{2-} \rightarrow Dy^{3+}$ interactions and host absorption band (HAB) and a series of sharp excitation lines in the 320-500 nm range, which are assigned to the intra- 4*f* transitions of the Dy^{3+} ions. These excitation peaks in longer wavelength region are located at 326, 353, 366, 388, 427, 453 and 470 nm corresponding to transitions of Dy^{3+} ions from $^6H_{15/2}$ energy state to $^6P_{3/2}$, $^6P_{7/2}$, $^6P_{5/2}$, $^4I_{13/2}$, $^4G_{11/2}$, $^4I_{15/2}$ and $^4F_{9/2}$ respectively, peak with maxima at 353 nm being the dominating [26].

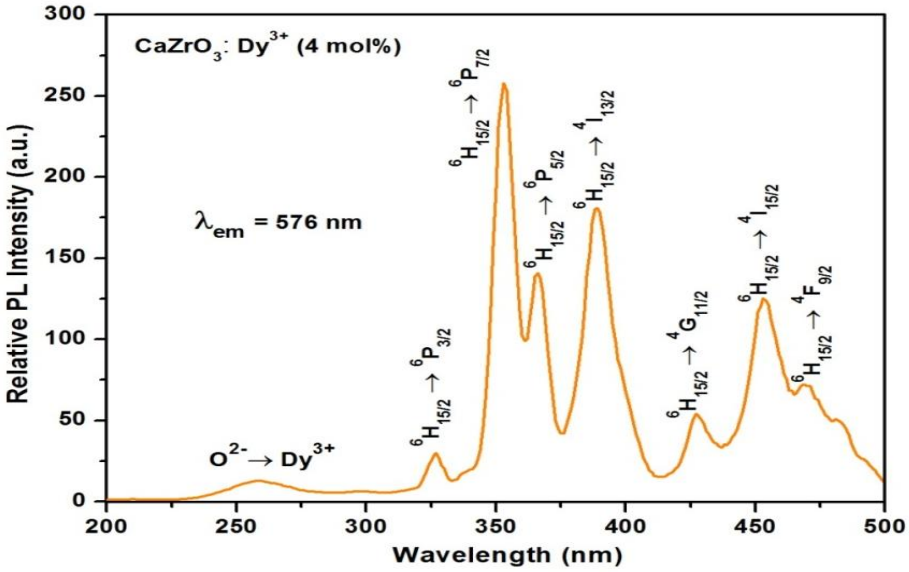

Fig. 4 Photoluminescence excitation (PLE) spectrum of $Ca_{0.96}Dy_{0.04}ZrO_3$ nanophosphors sintered at 1200°C, monitored with λ_{em} = 576 nm

The photoluminescence (PL) spectra of $Ca_{0.96}Dy_{0.04}ZrO_3$ nanophosphors as-synthesized and sintered at different temperatures, monitored at 353 nm excitation in 425-675 nm region is depicted in Fig. 5. The PL spectra consist of two sharp emission lines in the blue region (470-490 nm) and yellow region (530-650 nm). The blue emission centered at 484 nm corresponds to $^4F_{9/2} \rightarrow {}^6H_{15/2}$ while yellow emission with maxima at 576 nm is ascribed $^4F_{9/2} \rightarrow {}^6H_{13/2}$ transitions of Dy^{3+} ions, respectively [21].

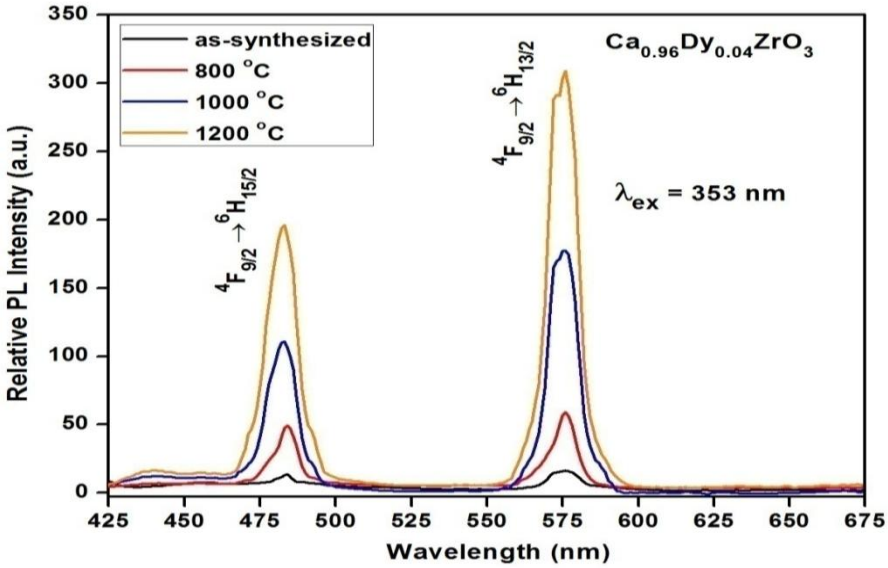

Fig. 5 Photoluminescence (PL) spectra of $Ca_{0.96}Dy_{0.04}ZrO_3$ nanophosphors sintered at different temperatures, monitored with λ_{ex} = 353 nm

It is quite apparent that relative PL intensity of yellow emission ($^4F_{9/2} \rightarrow {}^6H_{13/2}$) corresponding to forced electric transition is stronger than that of blue emission ($^4F_{9/2} \rightarrow {}^6H_{15/2}$) belonging to magnetic dipole transition. Being hypersensitive yellow emission with the selection rule, $\Delta J = 2$, get greatly influenced by the outside surroundings while blue emission is hardly influenced by crystal field symmetry of Dy^{3+} ions [27]. Increase in PL intensity of as-synthesized $Ca_{0.96}Dy_{0.04}ZrO_3$ nanophosphors corresponding to both blue and yellow transitions with the rise in sintering temperature from 800 to 1100°C is quite visible. This may be attributed to reduction in non-radiative recombination effects, quenching sites and surface defects in the crystal structure at higher temperature, hence leading to improvement in doping and better crystallinity [28].

The PL spectra of $Ca_{1-x}Dy_xZrO_3$ doped with different Dy^{3+} contents sintered at 1200°C, monitored at 353 nm excitation are illustrated in Fig. 6. Variable contents of dysprosium ions have no distinct influence on the shape and positions of emission lines in PL spectra. In all $Ca_{1-x}Dy_xZrO_3$ samples, hypersensitive yellow ($^4F_{9/2} \rightarrow {}^6H_{13/2}$) emission was found to be greater than blue ($^4F_{9/2} \rightarrow {}^6H_{15/2}$) emission. However, increase in the relative PL intensities corresponding to both transitions with increasing dysprosium concentration was noticed. The maximum emission intensity was observed at 4 mol% of Dy^{3+} ions contents in $Ca_{1-x}Dy_xZrO_3$ nanophosphors and decreased afterwards owing to well-known concentration quenching phenomenon. This concentration quenching may be attributed to the non-radiative cross relaxation process between adjacent Dy^{3+} ions at higher concentration, causing depopulation of the $^4F_{9/2}$ energy state of Dy^{3+} ions as; Dy^{3+} ($^4F_{9/2}$) + Dy^{3+} ($^6H_{15/2}$) → Dy^{3+} ($^4F_{9/2}/{}^6H_{7/2}$) + Dy^{3+} ($^6F_{3/2}$) [33, 29]. In addition, constant yellow to blue emission ratio (Y/B~1.5) with the increasing Dy^{3+} contents in $CaZrO_3$ lattice leads to assume that the hypersensitive electric forced transition ($^4F_{9/2} \rightarrow {}^6H_{13/2}$) senses no remarkable variation in the crystal field symmetry of Dy^{3+} ions in this pervoskite $CaZrO_3$ lattice.

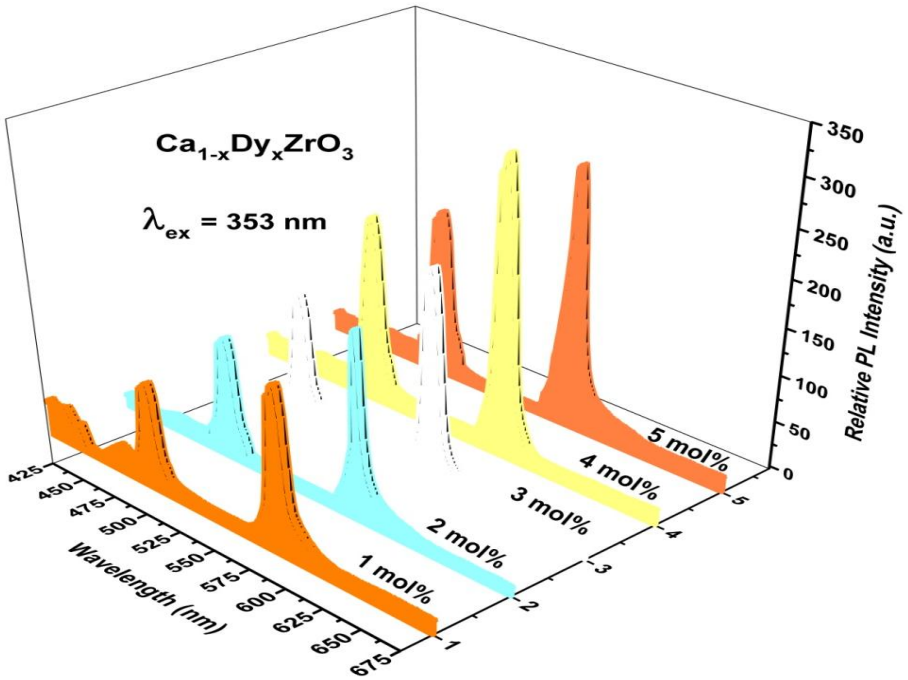

Fig.6. Photoluminescence (PL) spectra of $Ca_{1-x}Dy_xZrO_3$ powders doped with different dysprosium contents sintered at 1200°C and monitored at λ_{ex} = 353 nm.

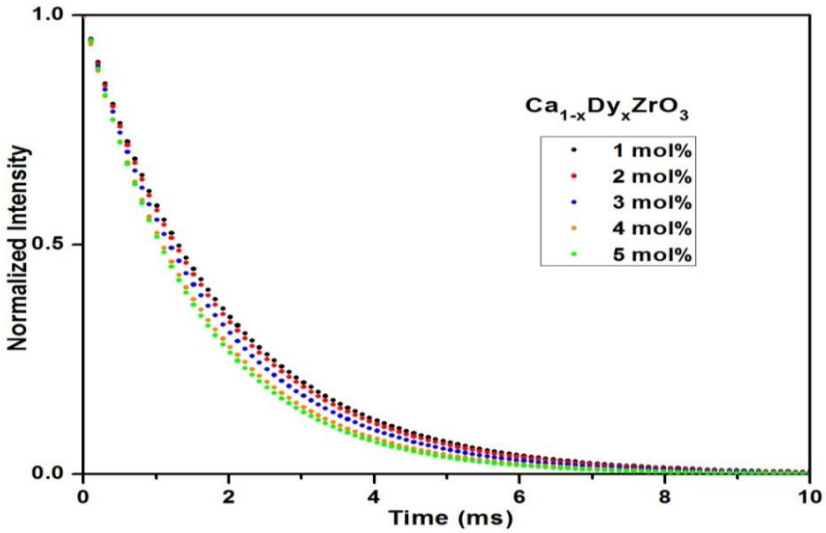

Fig. 7 Decay curves $Ca_{1-x}Dy_xZrO_3$ powders doped with different dysprosium contents sintered at 1200°C, monitored at λ_{ex} = 353 nm and λ_{em} = 576 nm

The luminescence decay curves for $Ca_{1-x}Dy_xZrO_3$ nanophosphors where x = 0.01 to 0.05 corresponding to yellow emission ($^4F_{9/2} \rightarrow {}^6H_{13/2}$) monitored at 353 nm excitation ($^6H_{15/2} \rightarrow {}^6P_{7/2}$) are displayed in Fig. 7. All the decay curves were found to be mono- exponential, represented by the equation $I = I_0 \exp(-t/\tau)$, where τ is the radiative decay time, I and I_0 are the luminescence intensities at time t and 0, respectively. The calculated average lifetimes for 0.5, 1, 3, 4, 5 and 7 mol% of Dy^{3+} ions in $Ca_{1-x}Dy_xZrO_3$ nanophosphors are 1.88 ms, 1.82 ms, 1.71 ms, 1.57 ms and 1.50 ms, respectively. This decrease in average lifetimes with the increasing dysprosium contents may also be due to enhanced non-radiative energy transfer between dopant ions at higher concentration. The Commission International De I'Eclairage (CIE) chromaticity coordinates for $Ca_{1-x}Dy_xZrO_3$ nanophosphors doped with 0.1 to 5 mol% dysprosium contents were calculated from their corresponding PL spectra, monitored with 353 nm excitation and represented in Fig 8. The color coordinates (x, y) of $Ca_{1-x}Dy_xZrO_3$ samples located at (0.360, 0.371), (0.330, 0.348), (0.333, 0.365), (0.348, 0.379) and (0.367, 0.366) for 1, 2,3, 4 and 5 mol%, respectively are found to be very close to the standard color systems such as ProPhoto/Color Match (0.3457, 0.3585) and CIE white light point (0.33, 0.33) [30]. It is quite apparent that white light is slightly tending towards yellowish hue with the increasing dysprosium concentration in $Ca_{1-x}ZrO_3$ nanophosphors.

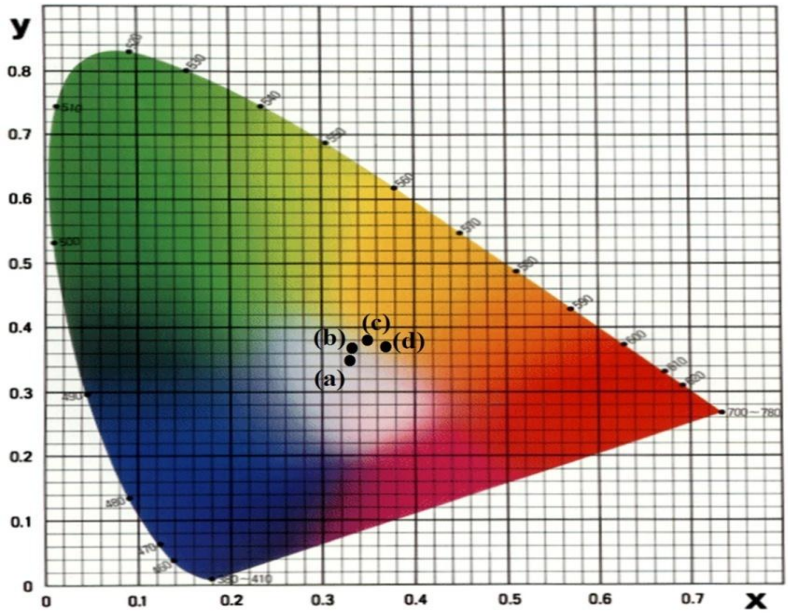

Fig. 8 CIE color (*x*, *y*) coordinates for (a) 2 mol%, (b) 3 mol%, (c) 4 mol%, and (e) 5mol%, of Dy^{3+} ions in $Ca_{1-x}Dy_xZrO_3$ nanophosphors sintered at 1200°C after excitation at 353 nm

Conclusion:

In brief $CaZrO_3$: Dy^{3+} nanophosphors have been successfully synthesized by urea assisted solution combustion method and their structural as well as luminescent characteristics were studied for various sintering temperature and dysprosium concentration. Highly crystalline single phased $Ca_{1-x}Dy_xZrO_3$ at 1200ºC as revealed by X-ray diffraction studies. Morphological analysis of these dysprosium doped powders indicates narrow distribution of highly crystalline particles in nano-regime. Luminescent features of $Ca_{1-x}Dy_xZrO_3$ nanophosphors were studied in details using photoluminescence excitation (PLE) and photoluminescence emission (PL) alongwith luminescence decay curves and color (*x*, *y*) coordinates in order to determine the exact optimal conditions for superior luminescence. Several characteristics sharp excitation peaks attributed to intra-4*f* transitions of the Dy^{3+} ions in 300-500 nm range were observed. The dependence of the emission intensity of $Ca_{1-x}Dy_xZrO_3$ nanophosphors on the *x* value has also been investigated and found to be maximum at 4 mol% of dysprosium ions. $Ca_{1-x}Dy_xZrO_3$ nanophosphors are potential candidates for white light emission which may be achieved by proper tuning of yellow to blue emission intensities on varying the composition of host.

REFERENCES

1. V. Singh, S. Watanabe, T.K. Gungu Rao, K. Al-Shamery, M. Haase, *J. Lumin.*, 132 (2012) 2036.
2. N. Pal, M. Paul, A. Bhaumik, *Appl. Catal. A*, 393 (2011) 153.
3. R. Parra, R. Savu, L.A. Ramajo, M.A. Ponce, J.A. Varela, M.S. Castro, P.R. Bueno, E. Joanni, *J. Solid State Chem.*, 183 (2010) 1209.
4. Z. Lu, L. Chen, Y. Tang, Y. Li, *J. Alloys Compd.*, 387 (2005) L1.
5. W.Y. Jia, W.L. Xu, I. Rivera, A. Perez, F. Fernandez, *Solid State Commun.*, 126 (2003) 153.

6. F.H. Norton, *Fine Ceramics*, Mcgraw-Hill, New York, (1970) 40.
7. T. Yajima, K. Koide, H. Takai, N. Fukatsu, H. Iwahara, *Solid State Ionics*, 79 (1995) 333.
8. Y. Suzuki, P. E. D. Morgan, T. Ohji, *J. Am. Ceram. Soc*., 83 (2000) 2091.
9. S.K. Manik and S.K. Pradhan, *J. Appl. Crystallogr*., 38 (2005) 291.
10. Y. Suzuki, P.E.D. Morgan, T. Ohji, *Mater. Sci. Eng. A-Struct*., 304–306 (2001) 780.
11. A.M. Azad, S. Subramaniam, T.W. Dung, *J. Alloys Compd.*, 334 (2002) 118.
12. M. Pollet, S. Marinel, G. Desgardin, *J. Eur. Ceram. Soc.*, 24 (2004) 119.
13. K. Kiyoshi, Y. Shu, I.Yoshiaki, *Solid state Ion.*, 108 (1998) 355.
14. T. Yamagushi, Y. Komatsu, T. Otobe, Y. Murakami, *Ferroelectrics*, 27 (1980) 273.
15. G. Rog, M. Dudek, A. Kozlowska-Rog, M. Bucko, *Electrochim. Acta*, 47 (2002) 4523.
16. W. Engelen, A. Buekenhoudt, J. Luyten, A. D. Shutter, *Solid State Ion.*, 96 (1997) 55.
17. H. Iwahara, Y. Asakura, K. Katahria, M. Tanaka, *Solid State Ion*., 168 (2004) 229.
18. J. Kung, R.J. Angel, N.L. Ross, *Phys. Chem. Miner.*, 28 (2000) 35.
19. G.S.R. Raju, J.Y. Park, H.C. Jung, B.K. Moon, J.H. Jeong, J.H. Kim, *Curr. Appl. Phys.* 9 (2009) e92.
20. D. Gao, Y. Li, X. Lai, Y. Wei, J. Bi, Y. Li, M. Liu, *Mater. Chem. Phys*., 126 (2011)391.
21. S.D. Han, S.P. Khatkar, V.B. Taxak, G. Sharma, D. Kumar, *Mater. Sci. Eng. B*, 129 (2006)126.
22. C.R. Kesavulu, and C.K. Jayasankar, *Mater. Chem. Phys.*, 130 (2011)1078.
23. W. Li, G. Zhou, A. Zhang, Q. Du, H. Zhou, J. Zhang, *J. Chin. Ceram. Soc*., 39 (2011) 1729.
24. R. Vassen, X. Cao, F. Tietz, D. Basu, D. Stover, *J. Am Ceram. Soc.*, 3 (200) 2023
25. S. Ekambaram and K.C. Patil, *J. Alloys Compds.*, 448 (1997)7.
26. G.S.R. Raju, H.C. Jung, J.Y. Park, C.M. Kanamadi, B.Y. Moon, J.H. Jeong, S.-M. Son, J.H. Kim, *J. Alloys Compds.*, 481 (2009) 730.
27. J. Mulak and M. Mulak, *J. Phys A: Math Theor.*, 40 (2007) 2063.
28. Sonika, S.D. Han, S.P. Khatkar, M. Kumar, V.B. Taxak, *Mater. Sci. Eng. B*, 178 (2013) 1436.
29. L.A. Diaz-Torres, E.D.L. Rosa, P. Salas, V.H. Romero, A. Angeles-Chavez, *J. Solid State Chem*., 181 (2008) 75.
30. G.S.R. Raju, J.Y. Park, H.C. Jung, B.K. Moon, J.H. Jeong, J.H. Kim, *Curr. Appl. Phys.* 9 (2009) e92.